Dynamically Modulated GaN Whispering Gallery Lasing Mode for Strain Sensor

*Yiyao Peng, Junfeng Lu, Dengfeng Peng, Wenda Ma, Fangtao Li, Qiushuo Chen, Xiandi Wang, Junlu Sun, Haitao Liu, and Caofeng Pan**

The continuous development of strain sensors offers significant opportunities for improving human–machine interfaces and health monitoring. The dynamically modulated lasing mode is a novel approach to realize a flexible, noncontact, high color-resolvability, high-resolution, and ultrasensitive strain sensor. Here, a flexible strain sensor perceiving stress variations is reported via the dynamical regulation of a GaN whispering gallery lasing mode based on the piezoelectric effect. The refraction index of GaN shows a linear relationship with the applied external tensile strain, resulting in a redshift phenomenon of the lasing mode peak at room temperature due to the predominant function of the piezoelectric polarization in the GaN microwire. Compared with a strain sensor relying on the wavelength shift of a photoluminescence (PL) emission peak, the differences and advantages of a sensor based on the strain-induced lasing mode variation are also investigated and analyzed systematically. This strain sensor may serve as an essential step toward the color mapping of mechanical signals by optical methods, with potential applications in color-perceived touching sensing, noncontact stress measurement, laser modulation, and optical communication technologies.

1. Introduction

Strain sensors, as a hot research topic, are imperative for the development of infrastructural monitoring, robotic smart skin, human–machine interactive interfaces, and biomedical therapies.[1–4] After decades of efforts, strain sensors have been continuously developed toward high resolution, high sensitivity, rapid response, and flexibility, and the physical conduction mechanisms of strain sensors can be mainly summarized as resistance, capacitance, and piezoelectricity.[5,6] Since Wang proposed the field of piezotronics and piezo-phototronics, piezoelectric strain sensors have obtained increasing attention and development.[7,8] Pan et al. successfully fabricated a high-resolution and ultrasensitive pressure sensor array using oriented ZnO nanowires to effectively achieve 2D pressure-distribution mapping.[9] Subsequently, a series of flexible piezo-phototronic pressure sensors based on a ZnO nanowire/PEDOT:PSS light-emitting diode (LED) array, CdS nanorod/organic-hybridized LED array and transferred Si microwire/ZnO nanofilm has been successively reported by our group due to the demands of artificial skin for flexibility.[10–12] To further accomplish a higher resolution, better stability, and longer lifespan, a flexible p-GaN/n-ZnO nanowire LED-based pressure sensor array is prepared through a GaN-film laser lift-off process and ZnO-nanowire hydrothermal growth.[13] Notably, all the pressure distribution mappings are acquired by reading the change in each LED pixel illumination intensity, which is affected by many factors, such as the surrounding lighting condition and an uneven current density. Compared with the change in emission intensity, few external elements can influence the wavelength, providing an opportunity to exploit a more reliable and stable strain sensor.[14] Meanwhile, the noncontact detection method avoids complex device fabrication and technological processing and achieves strain sensing through optical signal acquisition, which broadens the application of strain sensors to scenarios such as liquid environments and remote stress detection.[10,15] Thus, the fabrication of a flexible, color-tunable and noncontact strain sensor is significantly important.

As for the strain sensor via dynamically regulating the emission wavelength to sense a mechanical stimulus, two kinds of different modulation mechanisms can be concluded as PL

Y. Peng, Dr. J. Lu, W. Ma, F. Li, Q. Chen, Prof. X. Wang, J. Sun, H. Liu, Prof. C. Pan
Beijing Key Laboratory of Micro-nano Energy and Sensor
Beijing Institute of Nanoenergy and Nanosystems
Chinese Academy of Sciences
Beijing 100083, P. R. China
E-mail: cfpan@binn.cas.cn

Y. Peng, Dr. J. Lu, W. Ma, Prof. X. Wang, Prof. C. Pan
School of Nanoscience and Technology
University of Chinese Academy of Sciences
Beijing 100049, P. R. China

Prof. D. Peng, Prof. C. Pan
College of Optoelectronic Engineering
Shenzhen University
Shenzhen 518060, P. R. China

J. Sun, H. Liu
Department of Physics and Laboratory of Materials Physics
Zhengzhou University
Zhengzhou 450001, P. R. China

Prof. C. Pan
Center on Nanoenergy Research
School of Physical Science and Technology
Guangxi University
Nanning 530004, P. R. China

The ORCID identification number(s) for the author(s) of this article can be found under https://doi.org/10.1002/adfm.201905051.

DOI: 10.1002/adfm.201905051

peak moving tuned by an external applied strain due to the piezoresistive effect and a strain-induced lasing mode variation based on the piezoelectric effect.[16,14] Initially, wurtzite-structured semiconductor materials were demonstrated to possess piezoresistivity and piezoelectricity, such as ZnO, CdS, GaN, etc., so several piezoelectric strain sensors have been designed and fabricated with these materials.[17,18] In recent years, the dependence of the shift of the near-band-edge (NBE) emission peak on external tensile and compressive strains in a ZnO cavity has been reported and is due to the effective change in the optical bandgap as tuned by the applied strain, which yields a means to deduce the magnitude of the applied stress.[19] However, the NBE emission variation-based strain sensors possess many critical drawbacks such as a low color-resolvability and low resolution. Recently, a novel method to obtain the value of applied strain using the evolution of lasing mode in ZnO microwires, CdS nanobelts or $CsPbBr_3$ microwires has been proposed.[14,20–22] Moreover, compared with these materials, GaN possesses a superior stability, high melting point, and wide energy bandgap, leading to wide application spaces such as short-wavelength, intense radiation, high temperature, and strong acidity or alkalinity situations.[23,24] Therefore, a flexible, noncontact, high-color resolving, and high-resolution strain sensor based on stable hexagonal GaN microwires needs to be constructed to meet the future extensive application requirements.

Here, we report a flexible strain sensor sensing a stress variation via the dynamical modulation of a GaN whispering gallery lasing mode, which is fabricated through chemical vapor deposition (CVD)-synthesized GaN microwires horizontally fixed on a polyethylene terephthalate (PET) substrate. When a tensile strain is applied by bending the PET substrate, the redshift in the lasing mode can be clearly observed owing to the intrinsic piezoelectric polarization effect of GaN. Moreover, the dependence of the lasing peak wavelength variation on the applied strain shows a linear relationship, indicating that not only can the whispering gallery lasing mode be regulated through mechanical stimuli but also the magnitude of applied strain can be confirmed according to the wavelength variation of the lasing mode. Compared with the shift in the strain-induced photoluminescence (PL) emission peak, the strain sensor based on the lasing mode change possesses an excellent color-resolvability and a high resolution owing to the higher color purity of lasing, which can detect a minimum strain change of 0.16%. Additionally, the inner mechanism of the piezoelectric polarization effect and Raman spectra of GaN are also investigated, clarifying that the piezopotential enhances with the external applied tensile strain resulting in an increase in the refractive index of the GaN microcavity. The strain sensor, exhibiting many advantages including flexibility, high color-resolvability, noncontact interactions, high resolution, and a simple construction, could be a significant step in the fields of noncontact stress measurement under extreme conditions, long-range strain detection, color-tunable pressure mapping, and optical signal modulation.

2. Results and Discussion

The strain sensors are fabricated by a simple technological process combining directional transfer and fixed encapsulation, as indicated in Figure S1a in the Supporting Information. A complete test system is shown in **Figure 1**a, which consists of a set of confocal microscopes equipped with an emission collection system including a spectrograph and charge-coupled device (CCD) detector coupled with a λ_{ex} = 350 nm pulsed laser, with a pulse duration of 190 fs, as an excitation source. A homemade manual displacement stage was designed and utilized as the device to apply stress. To investigate the corresponding relationship between emission spectra and mechanical stress, the optical performance of the GaN microwires under different applied strains was detected by the light-force coupling measurement system. Figure 1b presents a schematic diagram of the strain sensor, revealing numerous merits such as high resolution (in comparison to the strain-loaded NBE emission), flexibility, high color-resolvability, noncontact interactions, and a simple construction. When an external tensile strain is applied to the GaN microwire, the refractive index of the microresonator becomes tuned, thereby accomplishing the dynamical modulation of the lasing mode. To realize the crystal structure, the X-ray powder diffraction (XRD) pattern of as-grown GaN microwires is displayed in Figure 1c, from which we can observe that all the diffraction peaks match well with the characteristic peaks of the wurtzite phase of GaN (JCPDS no. 50-0792). The inset shows the wurtzite structure of GaN with a hexagonal system. The morphology of the as-grown GaN microwire is revealed in an scanning electron microscope (SEM) image (Figure 1d), with a diameter of ≈3 μm and a length of approximately a few hundred micrometers, the inset of which displays an optical image of the strain sensor with the GaN microwire fixed on the PET substrate by an epoxy resin to avoid slippage under the applied strain. Moreover, transmission electron microscopy (TEM) was used to further characterize the crystalline phase of the GaN microcavities. Figure 1e shows the element mapping images collected from the white rectangle region, in which Ga and N elements are uniformly distributed and the outline can be clearly observed. The corresponding energy dispersive X-ray spectrum is provided in Figure S1b in the Supporting Information. According to the selected-area electron diffraction (SAED) pattern (Figure 1f), it can be concluded that the GaN microwire possesses a single crystal structure and high crystallinity with a growth direction along the [0001]. The highly crystalline phase of the GaN microcavity can be observed directly from the high-resolution transmission electron microscopy (HRTEM) image, with a plane spacing of 2.81 Å parallel to the [0001] direction (Figure 1g). Accordingly, the hexagonal GaN microwire can act as a natural and high-quality cavity, in which the light can propagate constantly and maintain low energy loss through multiple total internal reflections at the inner walls, providing a possibility to obtain low-threshold and high-quality-factor whispering gallery mode (WGM) lasing. Meanwhile, GaN is an intrinsic and excellent optical gain medium. Upon excitation by a 325 nm continuous laser, a strong NBE emission peak centered at 370 nm and an extremely weak defect emission are shown in Figure S1c in the Supporting Information, which can offer sufficient optical gain for lasing.

To demonstrate the optical reliability of the GaN microcavity, a series of lasing spectra are acquired and analyzed at room temperature. **Figure 2**a indicates the typical emission spectra as a function of the average power from a single GaN microwire,

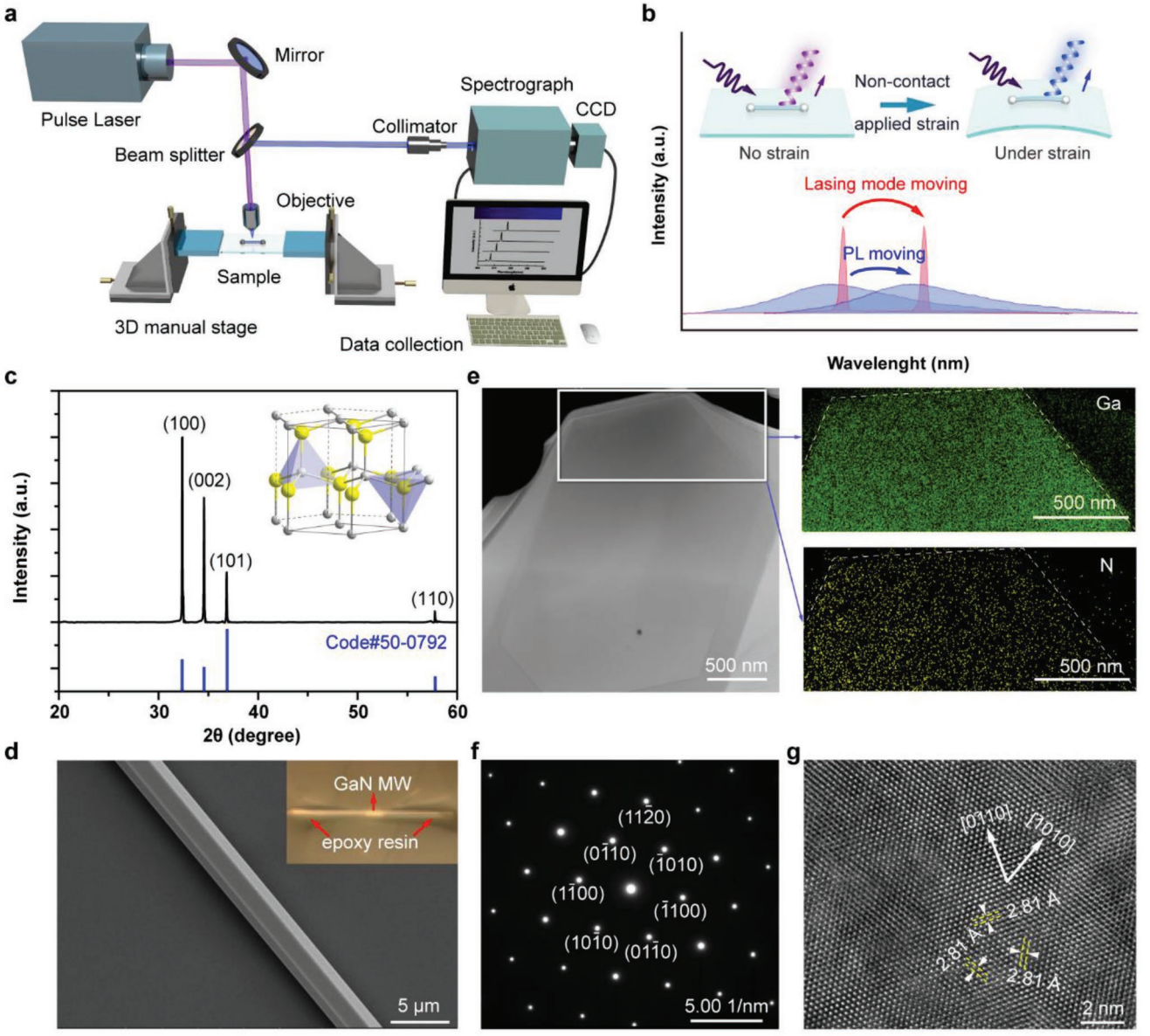

Figure 1. The complete test set, structural analysis, and morphology characterization of a GaN microwire. a) The optical path system for measuring the lasing mode moving in the GaN microcavity. b) A schematic diagram of the dynamically modulated GaN lasing mode with and without applied strain. c) The XRD pattern of an as-grown GaN microwire. The inset shows the crystal structure of wurtzite GaN. d) An SEM image of the top view of a single GaN microwire. The inset displays an optical image of the strain sensor GaN microwire fixed on the PET substrate by epoxy resin. e) Elemental mappings of Ga and N for hexagonal cross-sectional plane. f) SAED pattern of the GaN microwire indicating a single crystal structure. g) An HRTEM image of the as-synthesized GaN microwire.

the inset of which presents the corresponding 2D pseudocolor plot near the threshold. Only a weak and broad spontaneous emission peak centered at 366 nm can be observed at a low pumping power ($P \leq 2.65$ μW), and the corresponding full-width at half-maximum (FWHM) is ≈13 nm. With increasing pumping power to 2.83 μW, two sharp and discrete peaks appear from the broad spontaneous emission. More lasing peaks can be observed as the pumping power continues to increase, and the FWHM drops rapidly to ≈0.36 nm. Figure 2b displays the integrated PL intensity and FWHM plot as a function of the average power. According to the results of fitting the plots, the lasing threshold (P_{th}) equals ≈2.83 μW. When $P < P_{th}$, PL intensity increases slowly, and the FWHM retains a large and relatively stable value. When $P \geq P_{th}$, the PL intensity presents a sudden rise, and the FWHM shows a fast fall, which implies the transition from spontaneous emission to stimulated emission. Additionally, the power-dependent emission spectra for the same GaN microwire under the condition of 0.34% tensile strain are shown in Figure S2a in the Supporting Information. The integrated PL intensity and FWHM as a function of pumping power are displayed in Figure S2b in the Supporting Information giving a P_{th} of ≈3.05 μW (larger than P_{th} with no strain), which is attributed

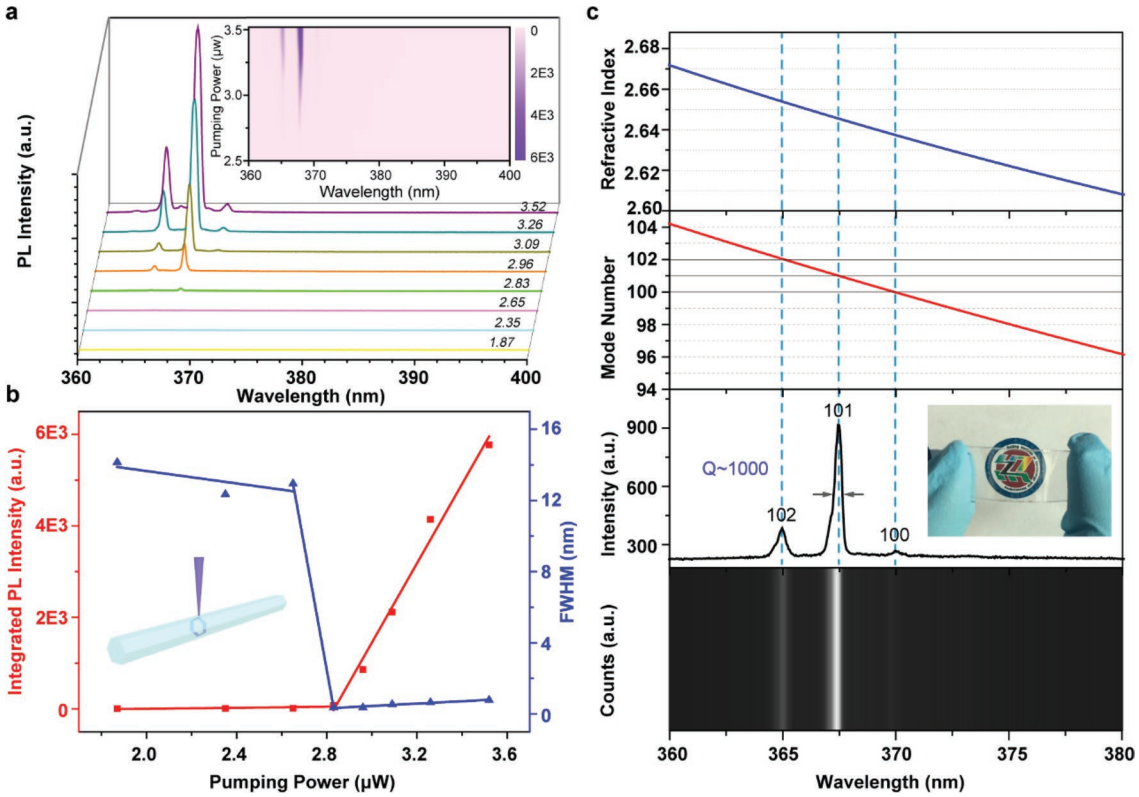

Figure 2. Lasing characteristics and mode analysis. a) Pumping-power-dependent lasing emission spectra for a GaN optical microcavity. b) The dependence of the integrated PL intensity and FWHM plot on the pumping power. The inset indicates the WGM in the GaN microcavity excited by a femtosecond laser at a wavelength of 350 nm. c) The confirmation of the whispering gallery lasing mode according to the corresponding relationship between the lasing peak and mode number. The inset shows an optical image of the flexible and transparent strain sensor.

to the piezoelectric polarization field decreasing the exciton binding energy of GaN to some extent due to the relatively small exciton binding energy GaN at room temperature (26 meV). Meanwhile, the lasing emission spectra and corresponding threshold curve of a thicker GaN microwire are also investigated, as indicated in Figure S3 in the Supporting Information. To further demonstrate the lasing resonant mode of the cavity, the characteristics of the lasing are analyzed, as presented in Figure 2c. In general, both TE and TM polarizations are involved in the lasing output. However, the TE-polarized emission is substantially stronger than the corresponding TM polarization, thus, only the TE mode is observed and analyzed in our work.[25,26] For TE polarizations, the refractive index of the lasing mode can be described as Sellmeier's dispersion function[27]

$$n(\lambda)=\left(3.60+\frac{1.75\lambda^2}{\lambda^2-0.256^2}+\frac{4.1\lambda^2}{\lambda^2-17.86^2}\right)^{1/2} \quad (1)$$

For a hexagonal WGM cavity, the corresponding relationship between the mode number (N) and resonant wavelength (λ) can be deduced by a plane wave model[28,29]

$$N=\frac{3\sqrt{3}nD}{2\lambda}-\frac{6}{\pi}\tan^{-1}\left(n\sqrt{3n^2-4}\right) \quad (2)$$

where n is the wavelength-dependent refractive index, and D is the cavity diameter. Figure 2c shows the lasing emission spectrum and corresponding intensity mapping image at a pumping power of 3.15 μW. The WGM TE mode numbers from 100 to 102 are calculated. The theoretical modes match quite well with the experimental resonant wavelengths, as listed in **Table 1**. Therefore, it can be concluded that the lasing behavior in our work is owed to the WGM resonant cavity. Additionally, the Q factor of the microcavity can also be acquired as ≈1000 according to the equation $Q=\lambda/\Delta\lambda$, where λ and $\Delta\lambda$ are the wavelength and FWHM of the lasing peak, respectively. The inset of Figure 2c shows an optical image of the flexible, transparent, and stable strain sensor.

To verify the lasing mode variation-based strain sensor possesses a higher resolution and detectivity than those of the PL moving detection, the lasing emission and NBE emission spectra for different tensile strains are measured, as shown in **Figure 3**a. The model and formula for calculating the applied strain achieved through bending samples are proposed in Figure S4 in the Supporting Information. When the tensile strain varies from 0% to 0.5% applied on the sensor, both the

Table 1. The theoretical and experimental lasing peak wavelength and calculated TE mode number.

N [Mode No.]	102	101	100
Theory [nm]	364.99	367.47	369.95
Experiment [nm]	364.96	367.47	369.97

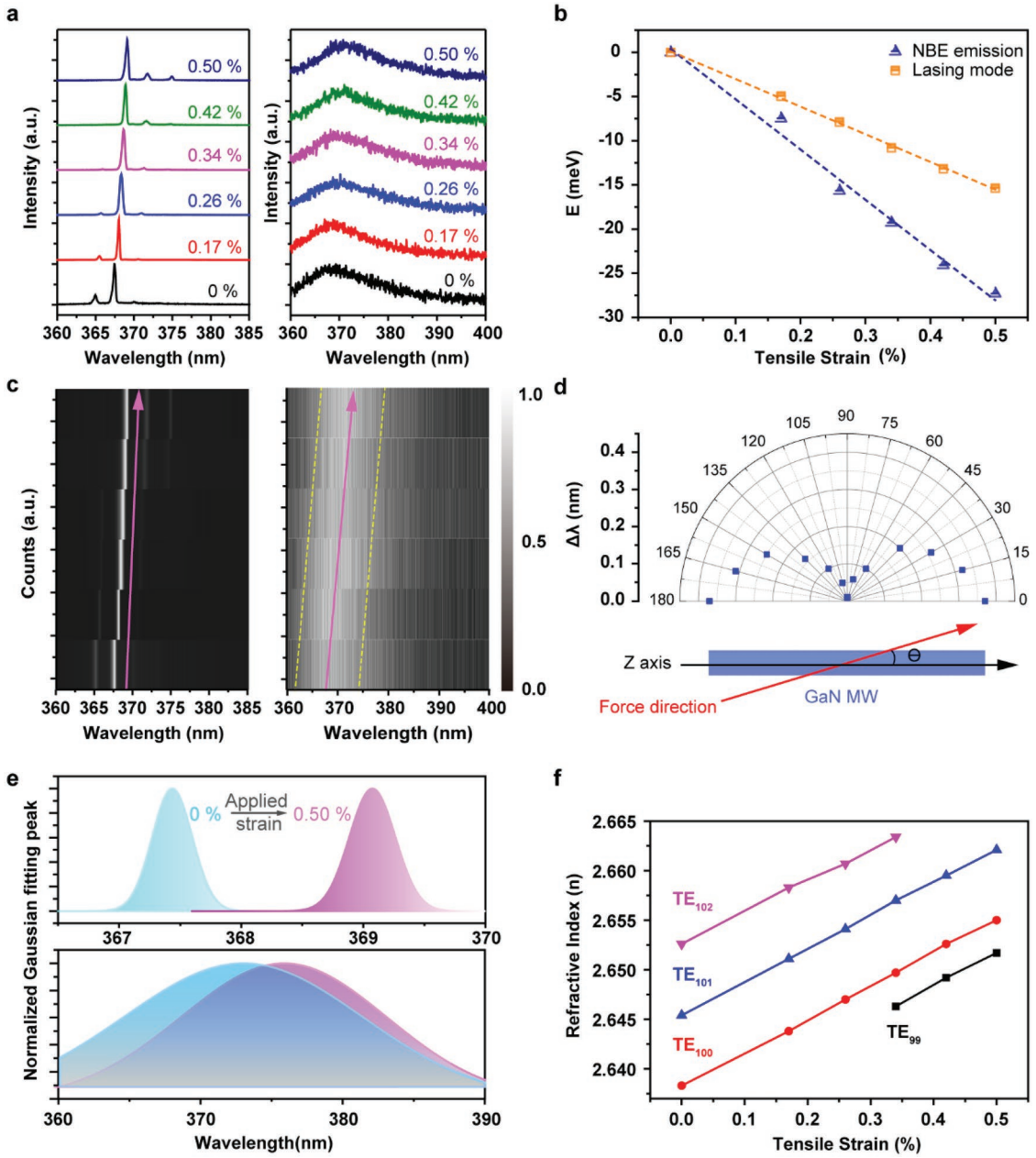

Figure 3. Dynamic modulation of the GaN whispering gallery lasing mode shift. a) Lasing and NBE emission spectra of the as-prepared GaN microresonator under different external tensile strains, and the corresponding mappings are shown in (c). b) The linear relationships between the variation in photon energy and applied tensile strain for lasing mode and NBE emission. d) The angle-dependent lasing mode variation for the same GaN microcavity. θ represents the included angle between the applied force direction and the GaN microwire *c*-axis direction. e) A higher color-resolvability and resolution for the variation in the lasing mode compared to that of the PL peak shift under a tensile strain of 0.50%. f) The refractive index as a function of applied tensile strain for different TE modes.

lasing peak and NBE emission peak produce redshift phenomena accompanied by the low-order mode emergence and the high-order mode disappearance. The normalized TE_{101} mode under different degrees of bending is displayed in Figure S5a in the Supporting Information. Notably, the inner mechanisms of the two kinds of spectral evolution show a great difference. The wavelength moving of the PL emission peak is caused by the strain-induced energy bandgap variation. However, the redshift in the lasing mode presented here can be attributed to the gradually increasing refractive index due to the growing crystal piezoelectric polarization induced by the strain. According to the Poisson ratio of GaN (≈0.352), the variations in diameter can be estimated as 3.32, 5.08, 6.64, 8.21, and 9.77 nm under tensile strains of 0.17%, 0.26%, 0.34%, 0.42%, and 0.50%, respectively. To exclude the effect of the cavity change under tensile strain on the lasing mode redshift, the mode wavelength, which only considers the influence of the cavity change, are calculated, as indicated in Table S1 in the

Supporting Information, where a slight blueshift contrary to the experimental redshift results can be observed. Thus, the piezoelectric effect does play a key role in the redshift phenomenon of the lasing mode. Figure 3b shows an approximately linear relationship (with R-squared greater than 0.99) between the peak wavelength variation and applied strain, indicating the redshift rate of the NBE emission peak is greater than that of the lasing mode peak with increasing applied strain, which further demonstrates the different underlying mechanisms of the two spectral evolutions. According to the reliable linear relationship, we can not only achieve dynamical and controllable modulation of the lasing mode by applying a corresponding stress but also detect the corresponding magnitude of the applied stress based on the shift in the resonant wavelength as a strain sensor. Moreover, compared to the PL emission, the lasing possesses a higher color purity; thus, we can imagine distinguishing the force distribution by color-tunable mapping. To quantitatively illustrate the sensor color-resolving ability (R), a model is proposed (Figure S5b, Supporting Information), and a formula with regard to the emission peak wavelength variation and FWHM is defined as

$$R = \left| \frac{\lambda_2 - \lambda_1}{\Delta H} \right| \tag{3}$$

where λ_1 and λ_2 stand for the lasing peak wavelengths before and after the applied stress, ΔH is the overlap in wavelength of the two lasing peaks and satisfies the functional relationship of $\frac{1}{\Delta H^2} = \frac{2}{\Delta \lambda^2} - \frac{2}{\omega^2}$ (ω and $\Delta\lambda$ represent the FWHM of the fitting curve and the actually measured lasing spectrum, respectively). When $R = 1$, the critical value is achieved whereby the two lasing peaks can be differentiated in distinguishable colors. $R > 1$ represents that the differentiation can be distinguished well as two kinds of colors, and $R < 1$ expresses the opposite situation. Moreover, the measured lasing modes under applied strains of 0.34% and 0.50% are analyzed and are demonstrated to be in a critical state whereby the two lasing peaks are just distinguishable, as shown in lower panel of Figure S5b in the Supporting Information. According to the theoretical model and linear relationship between wavelength variation and applied strain, the minimum strain resolution for the strain sensor is calculated as 0.14%, close to the experimental value of 0.16%.

To intuitively and clearly present the difference between the lasing mode moving and PL moving, the corresponding emission mappings with different degrees of tensile strain are shown in Figure 3c. Furthermore, the variation in the lasing peak relates to the force direction. The polar plot of Figure 3d indicates the lasing peak variation of the same ZnO microcavity versus the included angle between applied force direction and the GaN microwire *c*-axis direction. The distance of the wavelength shift appears as a sinusoidal function of the included angle from 0° to 90° under the same tensile strain, and the angle plot displays the axial symmetry along the *y* axis. The specific angle-dependent lasing spectra and corresponding wavelength shifts under different applied strains are shown in Figure S6 in the Supporting Information. Meanwhile, the diameter dependency of the GaN microwire lasing spectra are also investigated (Figure S7, Supporting Information). The number of lasing modes can be observed to increase and the mode spacing to decrease in the gain region with the increasing size of the resonant cavity. Figure 3e vividly reveals the spectral color-resolvability and resolution of the lasing mode-based sensor operated by a tensile strain higher than that of the PL-based strain sensor. As the tensile strain increases to 0.50%, most of the PL spectrum area is still overlapped with that under a tensile strain of 0%. Nevertheless, the lasing modes are completely separated for a distance under tensile strains of 0% and 0.50%. Accompanied by the redshift of the lasing peak wavelength (Figure S8a, Supporting Information), the linear relationship between the TE mode number and refractive index under different tensile strains can be fitted by fixing some relevant parameters, as shown in Figure S8b in the Supporting Information. Thus, the dependence of the refractive index of different lasing modes on the applied tensile strain is indicated in Figure 3f, revealing that the piezoelectric polarization effect plays a significant role in the refractive index. The greater influence of the piezoelectric polarization effect on the refractive index at the resonant frequency close to the bandgap energy distinctly clarifies the dominant reason for the change in the refractive index. The highly integrated microsystem and measurement device is constructed and used to characterize the optical performance of the strain sensor based on lasing mode moving in a GaN microcavity, as shown in Figure S9 in the Supporting Information.

To deeply investigate the intrinsic mechanism of the piezoelectric polarization effect in the GaN microwire, we analyze the crystal structure and the generation of the piezopotential in the GaN microcavity. The GaN wurtzite structure possesses both piezoelectric and semiconductor properties, where Ga^{3+} and the adjacent N^{3-} are tetrahedrally coordinated. The charge centers of the cations and anions overlap with each other under no pressure. When pressure is applied to the apex of the tetrahedron, the charge centers of the positive and negative ions are relatively displaced, and a dipole moment is generated, that is, a piezoelectric polarization effect occurs.[30] A constructive superposition of the dipole moments generated by all the elements in the crystal produce a macroscopic potential distribution along the force direction, as indicated in **Figure 4**a. To clarify that the applied force is uniaxial, Raman scattering spectra of the GaN microwire under different tensile strains are recorded. Figure 4b presents the Raman spectrum obtained without an applied strain, where the photon frequencies at 143, 530, 558, and 567 cm^{-1} are attributed to the E_2 (low), A_1 (TO), E_1 (TO), and E_2 (high) modes of the as-synthesized GaN microwire, respectively.[31,32] The strong and symmetric E_2 (high) phonon frequency implies the hexagonal phase property of a GaN microwire with high crystallinity. Upon gradually increasing the applied tensile strain, a significant redshift can be observed in the E_2 (high) phonon line, as shown in Figure 4c, while no evident change occurs to the A_1 (TO) phonon line under an applied tensile strain. This result can be ascribed to the tensile strain along the [0001] direction softening the E_2 (high) mode perpendicular to the stretching stress and enhancing the A_1 (TO) mode parallel to the applied stress direction (Figure 4d). Certainly, the Raman spectra of another sample are also acquired, and it indicates similar

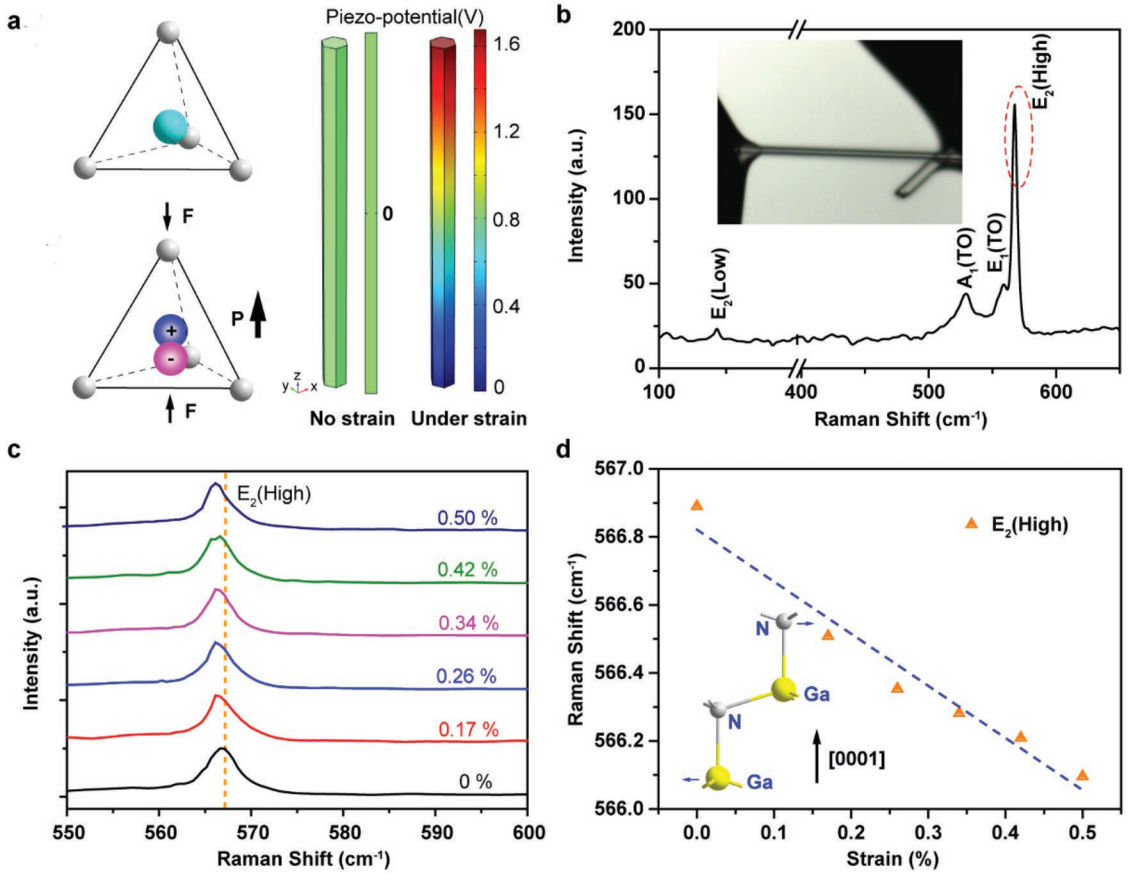

Figure 4. Mechanism analysis of the piezoelectric effect and Raman scattering spectra of the GaN microwire. a) An atomic structure model of the wurtzite GaN and the generation of a piezopotential along the *c*-axis direction of the GaN microwire, as calculated by numerical methods. b) Raman spectrum of the as-synthesized GaN microwire under no strain. The corresponding test sample is shown in the inset. c) The redshift phenomenon of the Raman E_2 (high) mode under increasing applied tensile strain. d) The Raman shift of the E_2 (high) mode as a function of the applied strain, the inset of which indicates the corresponding atomic vibrations.

characteristics (Figure S10, Supporting Information). Thus, uniaxial stress along the *c*-axis direction is applied to the sensor device.

3. Conclusion

In summary, we prepared a strain sensor based on the shift of a GaN whispering gallery lasing mode through the change in the refractive index of a microcavity caused by a continuously applied external mechanical stress, with the merits of flexibility, high resolution, superior color-resolvability, noncontact interactions, transparency, and a simple construction. The lasing spectra are tuned effectively by the external tensile strain due to the increase in the piezoelectricity-induced refractive index. When a tensile strain of 0.50% is applied, the lasing modes can be distinguished clearly, while most of the PL spectrum are remains overlapped with that under a tensile strain of 0%. The experimental minimum in strain resolution for the strain sensor reaches up to 0.16%. According to the reliable linear relationship between the wavelength variation of the lasing peak and the applied strain, we can not only modulate the lasing mode dynamically and controllably but also detect the corresponding magnitude of the applied stress as a high precision and flexible strain sensor. Our research represents a crucial step to the design and development of color-perceived touching/sensing micro/nanodevices, noncontact strain sensors, laser modulators, and photonic integrated circuits.

4. Experimental Section

Sensor Fabrication: High-quality GaN microwires, acting as the optical microcavity, were synthesized by the method of CVD, as introduced in the previous work.[33] Briefly, Ga_2O_3 powder, serving as the reaction source, and a GaN/sapphire substrate were put in an alumina boat covered by another alumina boat and then placed into the center of a tubular furnace to keep a reaction temperature of 1100 °C for 180 min under an atmosphere of NH_3 gas. Subsequently, the as-prepared GaN microwires were transferred onto the flexible PET substrate through dry adsorption and achieved control over their directionality via the probe. At last, the two ends of the GaN microwires were fixed on the PET substrate by an epoxy resin to ensure the tensile strain was applied to the microwires through the bend in the flexible substrate.

Structural Characterization: The morphology of the as-synthesized GaN microwires was characterized by a hot-field-emission SEM (Quanta 450). The crystal structure of the sample was analyzed with an X-ray diffractometer (PANalytical, X'Pert 3 Powder) with a Cu Kα

radiation source. Further structural characterizations were acquired by TEM (Titan ETEM G2) with a working voltage at 300 kV and equipped with energy-dispersive X-ray spectroscopy (EDS, EDAX Oxford X-Max) at a working voltage of 30 kV.

Optical Measurement: The corresponding relationships between the spectral shift and applied stress were characterized by a highly integrated microsystem. Specifically, a femtosecond pulsed laser, possessing a pulse duration of 190 fs and a repetition rate of 1 kHz, was employed to excite the samples at a wavelength of 350 nm. The spot diameter is 33.6 µm. The spontaneous and stimulated emission were collected through an optical multichannel analyzer (Andor, SR-500i-D1-R, 1200 g mm^{-1} grating) and a CCD detector coupled with a confocal µ-PL system (Zeiss M1). Raman spectra and PL full spectra were recorded by laser confocal micro-Raman system (LabRAM HR Evolution) with excitation wavelengths of 532 and 325 nm, respectively. The manual stage used for applying strain was homemade and could bend the flexible PET substrate by producing horizontal displacement.

Supporting Information

Supporting Information is available from the Wiley Online Library or from the author.

Acknowledgements

Y.P. and J.L. contributed equally to this work. The authors thank the support of national key R&D project from Minister of Science and Technology, China (2016YFA0202703), National Natural Science Foundation of China (Nos. 61805015, 51622205, 61675027, 51432005, 61505010, and 51502018), Beijing City Committee of Science And Technology (Z171100002017019 and Z181100004418004), Beijing Natural Science Foundation (4181004, 4182080, 4184110, and 2184131) and the "Thousand Talents" Program of China for pioneering researchers and innovative teams.

Conflict of Interest

The authors declare no conflict of interest.

Keywords

GaN microwires, lasing mode, piezoelectric effect, strain sensors, whispering gallery mode

Received: June 24, 2019
Revised: July 13, 2019
Published online:

[1] D.-H. Kim, N. Lu, R. Ghaffari, Y.-S. Kim, S. P. Lee, L. Xu, J. Wu, R.-H. Kim, J. Song, Z. Liu, J. Viventi, B. de Graff, B. Elolampi, M. Mansour, M. J. Slepian, S. Hwang, J. D. Moss, S.-M. Won, Y. Huang, B. Litt, J. A. Rogers, *Nat. Mater.* **2011**, *10*, 316.
[2] T. Yamada, Y. Hayamizu, Y. Yamamoto, Y. Yomogida, A. Izadi-Najafabadi, D. N. Futaba, K. Hata, *Nat. Nanotechnol.* **2011**, *6*, 296.
[3] H.-H. Chou, A. Nguyen, A. Chortos, J. W. F. To, C. Lu, J. Mei, T. Kurosawa, W.-G. Bae, J. B. H. Tok, Z. Bao, *Nat. Commun.* **2015**, *6*, 8011.
[4] Q. Hua, J. Sun, H. Liu, R. Bao, R. Yu, J. Zhai, C. Pan, Z. L. Wang, *Nat. Commun.* **2018**, *9*, 244.
[5] M. L. Hammock, A. Chortos, B. C. K. Tee, J. B. H. Tok, Z. Bao, *Adv. Mater.* **2013**, *25*, 5997.
[6] X. Wang, L. Dong, H. Zhang, R. Yu, C. Pan, Z. L. Wang, *Adv. Sci.* **2015**, *2*, 1500169.
[7] Z. L. Wang, *Adv. Mater.* **2007**, *19*, 889.
[8] Z. L. Wang, *Nano Today* **2010**, *5*, 540.
[9] C. Pan, L. Dong, G. Zhu, S. Niu, R. Yu, Q. Yang, Y. Liu, Z. L. Wang, *Nat. Photonics* **2013**, *7*, 752.
[10] R. Bao, C. Wang, L. Dong, R. Yu, K. Zhao, Z. L. Wang, C. Pan, *Adv. Funct. Mater.* **2015**, *25*, 2884.
[11] R. Bao, C. Wang, L. Dong, C. Shen, K. Zhao, C. Pan, *Nanoscale* **2016**, *8*, 8078.
[12] X. Li, R. Liang, J. Tao, Z. Peng, Q. Xu, X. Han, X. Wang, C. Wang, J. Zhu, C. Pan, Z. L. Wang, *ACS Nano* **2017**, *11*, 3883.
[13] Y. Peng, M. Que, H. E. Lee, R. Bao, X. Wang, J. Lu, Z. Yuan, X. Li, J. Tao, J. Sun, J. Zhai, K. J. Lee, C. Pan, *Nano Energy* **2019**, *58*, 633.
[14] J. Lu, C. Xu, F. Li, Z. Yang, Y. Peng, X. Li, M. Que, C. Pan, Z. L. Wang, *ACS Nano* **2018**, *12*, 11899.
[15] C. Wang, R. Bao, K. Zhao, T. Zhang, L. Dong, C. Pan, *Nano Energy* **2015**, *14*, 364.
[16] X. Han, L. Kou, X. Lang, J. Xia, N. Wang, R. Qin, J. Lu, J. Xu, Z. Liao, X. Zhang, X. Shan, X. Song, J. Gao, W. Guo, D. Yu, *Adv. Mater.* **2009**, *21*, 4937.
[17] R. Agrawal, H. D. Espinosa, *Nano Lett.* **2011**, *11*, 786.
[18] X. Wang, X. He, H. Zhu, L. Sun, W. Fu, X. Wang, L. C. Hoong, H. Wang, Q. Zeng, W. Zhao, J. Wei, Z. Jin, Z. Shen, J. Liu, T. Zhang, Z. Liu, *Sci. Adv.* **2016**, *2*, e1600209.
[19] X. Fu, Z. M. Liao, R. Liu, F. Lin, J. Xu, R. Zhu, W. Zhong, Y. Liu, W. Guo, D. Yu, *ACS Nano* **2015**, *9*, 11960.
[20] J. Lu, Z. Yang, F. Li, M. Jiang, Y. Zhang, J. Sun, G. Hu, Q. Xu, C. Xu, C. Pan, Z. L. Wang, *Mater. Today* **2019**, *24*, 33.
[21] W. Ma, J. Lu, Z. Yang, D. Peng, F. Li, Y. Peng, Q. Chen, J. Sun, J. Xi, C. Pan, *ACS Nano* **2019**, *13*, 5049.
[22] Z. Yang, J. Lu, M. ZhuGe, Y. Cheng, J. Hu, F. Li, S. Qiao, Y. Zhang, G. Hu, Q. Yang, D. Peng, K. Liu, C. Pan, *Adv. Mater.* **2019**, *31*, 1900647.
[23] J. F. Muth, J. H. Lee, I. K. Shmagin, R. M. Kolbas, H. C. Casey, B. P. Keller, U. K. Mishra, S. P. DenBaars, *Appl. Phys. Lett.* **1997**, *71*, 2572.
[24] K. Harafuji, T. Tsuchiya, K. Kawamura, *J. Appl. Phys.* **2004**, *96*, 2501.
[25] C. Czekalla, C. Sturm, R. Schmidt-Grund, B. Cao, M. Lorenz, M. Grundmann, *Appl. Phys. Lett.* **2008**, *92*, 241102.
[26] J. Dai, C. X. Xu, K. Zheng, C. G. Lv, Y. P. Cui, *Appl. Phys. Lett.* **2009**, *95*, 241110.
[27] J. Liu, S. Lee, Y. H. Ahn, J.-Y. Park, K. H. Koh, K. H. Park, *Appl. Phys. Lett.* **2008**, *92*, 263102.
[28] J. Wiersig, *Phys. Rev. A* **2003**, *67*, 023807.
[29] T. Nobis, M. Grundmann, *Phys. Rev. A* **2005**, *72*, 063806.
[30] Z. L. Wang, W. Wu, *Natl. Sci. Rev.* **2014**, *1*, 62.
[31] T. Azuhata, T. Sota, K. Suzuki, S. Nakamura, *J. Phys: Condens. Matter* **1995**, *7*, L129.
[32] V. Y. Davydov, Y. E. Kitaev, I. N. Goncharuk, A. N. Smirnov, J. Graul, O. Semchinova, D. Uffmann, M. B. Smirnov, A. P. Mirgorodsky, R. A. Evarestov, *Phys. Rev. B* **1998**, *58*, 12899.
[33] H. Liu, H. Zhang, L. Dong, Y. Zhang, C. Pan, *Nanotechnology* **2016**, *27*, 355201.